LUNDS UNIVERSITET
Naturvetenskapliga fakulteten

Bachelors Thesis Project

Division of Nuclear Physics

Department of Physics, Autumn 2021

Assessment of the Capability for Vetoing Beta-Decay Events in the Lundium Decay Station

Author
Tanvir Sayed

Supervisor
Luis G Sarmiento Pico

Co-Supervisor
Daniel M Cox

Examination
January 20, 2022

Abstract

Alpha decay spectroscopy using the latest and most sensitive detector setup as well as fast sampling read-out electronics has become very important for discovery and analysis of short-lived nuclei created in collision experiments in the laboratory. The Nuclear Structure Group in Lund is currently developing the Lundium Decay Station for use in comprehensive nuclear spectroscopy of decays for rare isotopes, particularly in the heavy & superheavy region. In this thesis work, the performance of the veto detector in the Lundium decay station is investigated to observe how well the implantation detector can distinguish low energy signals of to-be-reconstructed alpha particles from beta particles passing through. To investigate this, a ^{207}Bi source was used to radiate electrons on an implantation plus veto detector, back-to-back, setup at a distance very close to the face of the implantation detector. Data on the number and position of energy depositions (hits) recorded on both of them are analysed and used to build distributions of the electrons spread on the veto detector while 'gating' on pixels hit on the implantation detector. This very important finding allows one to determine how far apart hits on the two detectors can be for a beta particle passing through and still be considered to be from that same particle; this is becoming increasingly important as more (and new) fine structure of the alpha decays is investigated. The standard deviations calculated for the veto detector hit distributions, that can then be used to set electron hits apart in actual experiments to a suitable confidence level, was found to be about 4 mm.

Popular abstract

To identify and analyse the heavy and superheavy nuclei created in the lab, one measures a sequence or 'chain' of so-called decays, where often a charged 'alpha' particle – i.e a group of 4 nucleons – is ejected out from the nuclei. Beta decay is another type of decay where lighter, charged beta particles – electrons – are emitted, and as a result there are situations when it is necessary to distinguish between the incorrectly detected alphas and the betas. To solve this mystery, two charged particle detectors are used in a back-to-back set-up (the first known as 'implantation' while the second 'veto') to observe charged particles incident on them. Alphas are only picked out in 'photos' taken , referred to as hits, by the implantation detector, while electrons are able to be seen using both. However, there can be times when the fast electrons are emitted from the nuclei at a very sharp angle that it acts sneaky and is detected in the veto detector at a position not coincident with the detection position in the implantation detector. Thus, it becomes an issue to label the particle as an electron or an escaping alpha. To tackle this issue, an electron source – so there are no alphas to worry about and any hits not coincident in position are still caused only by the electrons – is used to irradiate the implantation and veto detector setup. By looking at the spread of the electron hits on the veto detector for certain selected 'pixel' hits – i.e. hit positions – on the implantation detector, one can determine how far the hits on the two detectors can be for identifying an impostor alpha, i.e. labeling the incoming particle as an electron.
This investigation, which is the first of its kind in house, will improve identification and analysis of the rare heavy and superheavy isotopes, making them more accurate and ensuring that no false alpha are being considered in the decay chains determined.

Acknowledgments

Firstly, I would like to give my greatest appreciation to my supervisor Pico who has been an excellent mentor throughout this project and has always made the subject very enjoyable and interesting. Next, I would give my thanks to Danny for helping me with the models in Fusion 360, setting up the experimental chamber for the experiment, as well as helping me fix and improve the grammar, spellings and formatting in my report. Special thanks to Dirk and Pavel for corrections of the different sections on my report drafts and more to Pavel for giving me all the necessary knowledge for the detectors and electronics being used. It was always nice and comforting to get the kind and motivating words from my seniors Yuliia and Dalia, helping greatly in not losing a fuse in my head. Last but not the least, many great thanks to Eli who has been the best companion along this thesis journey, in studies, stress and fika :).

Finally, thanks to everyone who was part of the NSG for making this thesis work a very enjoyable and memorable experience.

Contents

1 Introduction

This report covers the Bachelor of Science (BSc) thesis project work performed as part of the Nuclear Structure Group (NSG) in Lund in testing one of the many aspects of the newly designed 'Lundium Decay Station', more specifically testing the performance of Lundium in vetoing beta-decay events. Lundium is being developed by the group for investigating rare, exotic isotopes, in particular the heavy & superheavy ones at the far end of the nuclidic chart as highlighted in Fig. 1. Characterization and assessment of different components of the decay station are crucial to be carried out before the onset of using Lundium in decay spectroscopy experiments of scarcely produced short lived nuclei; this will enable all the necessary detector parameters to be known and ensuring the station works as best as it can from the start. The thesis work covered in this writing 'Assessment of the Capability for Vetoing Beta-Decay Events' is part of this comprehensive preliminary work on developing Lundium, and this dedicated study is also the first of its kind in house that will allow distinguishing low energy signals of escaping alpha particles from those of beta particles, with a known confidence level; in past experiments, vetoing has been carried out without a determination of this confidence level and simply labeling any such signals that reach the veto detector as '*not an alpha*'.

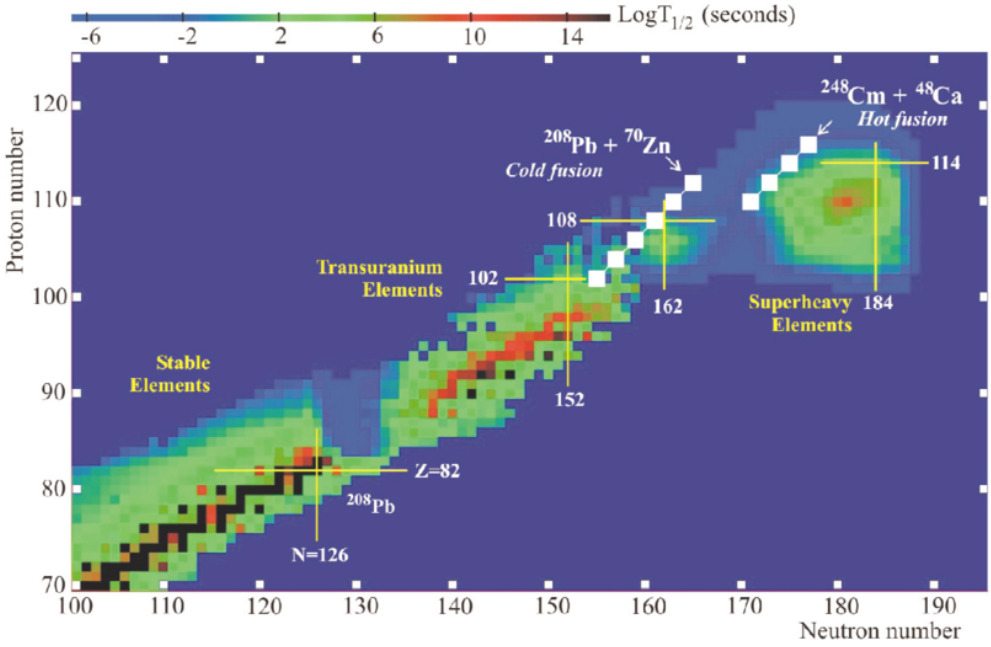

Figure 1: Section of the nuclidic chart containing the heavy & superheavy region. The timescale shown represents the lifetime of the isotopes. The white boxes illustrate decay chains for isotopes produced in the cold and hot fusion reactions shown [1].

All matter in the Universe is composed of tiny building blocks known as 'elements'. Every element, identified by their proton number, has distinct properties which eventually determine the characteristics of the matter it constitutes. In nuclear physics, one tries to unravel mysteries regarding the nuclei of all elements. One exciting area of nuclear physics is the study of the aforementioned heavy and superheavy elements. These nuclei are very short-lived and thus, it becomes very challenging to transmit them through separators into the detectors

after creation in experiments in a time span as small as a few microseconds. However, with newly developed advanced spectroscopic instruments – such as Lundium – to observe their decay chains, validation of their creation as well as properties of these quickly vanishing nuclei can be determined.

Creation of these exotic isotopes involve colliding two selected nuclei of specific atomic (proton) numbers such that the compound nuclei formed on impact is, at least close to, the one that is of interest. Typically, a beam of a 'lighter' nuclei is bombarded onto a rotating target wheel made of the second nuclei. The resulting compound nuclei can be further carried with the beam away from the target site. A separator is used to pass a 'filtered' beam, likely containing an isotope of interest, along to the decay station. An implanted nuclei in the decay station decays emitting ionizing radiation, for example by alpha radiation. At times, the alpha particles can escape back in the beam line producing a low energy signal potentially similar to an electron event. The process of vetoing aids to figure out the identities of the particles producing such low-signal events. In Lundium, a back-to-back setup of two double-sided silicon-strip detectors (DSSDs), one upstream for implantation and a second behind it for vetoing. Electrons may have enough penetration power to move through the implantation DSSD (often referred in this writing as 'IMP') to the second 'Veto' DSSD. However, the alpha particles do not and can not reach the Veto DSSD due to their low penetration power. This means that it is possible to distinguish and to reconstruct these alpha decays from the beta events. An important question that arises is 'how far apart can the positions of the energy depositions from beta particles in the two DSSDs be for labelling the event as one stemming from the same beta particle?'. This is exactly the main question that is studied in this thesis work.

This BSc thesis starts introducing the key concepts relevant to the thesis work, including the way ionizing radiation is produced and interacts with matter, and how these radiation can be detected with the help of semiconductor detectors. The structure of the Lundium decay station is discussed and in particular, a closer look is taken at its veto detector. The theory section is followed by the experimental methodology, the results produced by data analysis and a discussion of them. This report concludes with a summary of the work and findings as well as an outlook for related future studies.

2 Radiation-Matter Interactions

2.1 Origin of Ionizing Radiation

The origin of ionizing radiation, which are propagating charged particles or sufficiently energetic electromagnetic radiation, can be both natural (such as from cosmic rays and radon in Earth's bedrock) or artificial (during collision experiments in the laboratory). In most cases, ionizing radiation is due to unstable, radioactive nuclei in a state which by losing energy in some form would reach a more stable, lower energy state. The nucleus of any element consists of nucleons – positively charged protons and neutral neutrons – which are held together in a balance of an attractive nuclear force and repulsive Coulomb force between

them. The numbers of both kinds of nucleons in a nucleus are important. When a nucleus has too many of one type, the nucleus will become unstable and decay; the numbers of one or both kinds of nucleons, or the excitation energy of the nucleus, or both will change.

The unstable nuclei can undergo different kinds of radioactive decays where the mass of the parent nucleus is transferred into the mass and kinetic energy of the daughter nucleus (or nuclei if there are more than one) and emitted particles or photons. These radioactive decays primarily include alpha decays, beta decays, gamma decays or spontaneous fission [2]. For any decay process to be energetically feasible, the total mass of the daughter nuclei need to be lower than the total mass of the parent. This difference in total energy is known as the Q-value of the decay and also corresponds to the total kinetic energy of the decay fragments; typically, the more positive the Q-value, the more likely the decay. Additionally, in the process the conservation of mass-energy, momentum, and charge must always be followed. In the rest of this section, some of these common decay methods – namely alpha, beta and gamma decay – shall be presented.

2.2 Radioactive Decays

A common form of radioactive decay in which a positively charged particle is emitted is alpha decay. For nuclei with an excess of both protons and neutrons, the strong but short-range nuclear force is unable to counterbalance the repulsive, infinite range electromagnetic force. The parent nucleus tries to reduce its size, making the attractive nuclear force stronger, by emitting some of the nucleons as a small nucleus. This small nucleus is usually a helium nucleus – 2 protons and 2 neutrons, more commonly called an alpha particle – since the $Q-$value for this 'alpha decay' is higher than when emitting other nuclei [3]. For a parent nucleus X – with proton number Z, neutron number N, nucleon/mass number A – and daughter nucleus Y, the alpha decay can be represented as

$$ {}^{A}_{Z}\mathrm{X}_{N} \;\rightarrow\; {}^{A-4}_{Z-2}\mathrm{Y}_{N-2} + {}^{4}_{2}\,\mathrm{He}_{2}. \tag{1} $$

Its $Q-$value is the energy released in the reaction and corresponds to the kinetic energy of both decay fragments but since the alpha particle has much lower mass than the other daughter nucleus, most of the $Q-$value energy (usually $\approx 98\%$) goes to the kinetic energy of the alpha particle [3]. Charged particles like alpha particles with relatively high mass and charge, compared to electrons, are very likely to interact with matter as they propagate through it; hence, the radiation is short-ranged. This occurs mainly through the Coulomb interaction with the electrons in the matter, knocking the electrons from the atom in the material out and thus ionising the material. The kinetic energy of the alpha particles will reduce with each interaction. The mean energy loss per unit length in the material is given by the Bethe-Bloch formula [3].

$$ \left\langle \frac{dE}{dx} \right\rangle = \left(\frac{e^2}{4\pi\epsilon_0} \right)^2 \frac{4\pi Z_\alpha^2}{m_e c^2 \beta^2} \frac{Z N_A \rho}{A} \cdot \left[\ln\left(\frac{2 m_e c^2 \beta^2}{I\left(1-\beta^2\right)} \right) - \beta^2 \right]. \tag{2} $$

In Eq. 2, e is electron charge, ϵ_0 is the vacuum permittivity, N_A is the Avogadro's constant, m_e is the electron mass, ρ is density of the material, I is average excitation energy of the

electrons in the material, β is relativistic velocity, T_α is the kinetic energy of the α particle, m_α is the alpha mass, Z_α is the alpha atomic number, A is the mass number of the material, and Z is the proton number of the material.

A second decay process which involves emission of charged particles is 'beta decay'. For nuclei having an excess of either protons or neutrons, the parent nuclei will convert one of the excess nucleons into the other type and emit an electron or positron, respectively, along with an electron (anti-)neutrino to conserve momentum, spin and lepton number [2]. This emitted electron or positron in a beta decay is known as a beta particle. The beta minus decay – emission of electron – and beta plus decay – emission of positron – reactions are

$$ {}^{A}_{Z}\mathrm{X}_N \rightarrow {}^{A}_{Z+1}\mathrm{Y}_{N-1} + \beta^- + \bar{\nu}_e \quad \text{and} \tag{3} $$

$$ {}^{A}_{Z}\mathrm{X}_N \rightarrow {}^{A}_{Z-1}\mathrm{Y}_{N+1} + \beta^+ + \nu_e, \tag{4} $$

where β^- and β^+ represent electron and positron, while $\bar{\nu}_e$ and ν_e represent electron anti-neutrino and electron neutrino, respectively. Since these are three-body decays, the beta particles will have a continuous distribution of energies.

Electrons and positrons are charged particles and with enough energy (which are the ones commonly detected) will interact with matter causing ionisation. However, due to much smaller mass of the betas (and exactly the same as the electrons they knock off), the betas scatter in the material much more (Coulomb scattering) than alphas. The beta particles emitted may also travel at relativistic speeds. On collisions with the electrons in the material, the betas will undergo large energy losses and go through large deflections. This will lead to energy loss not only by Coulomb scattering but also by bremsstrahlung, where the rapid changes in direction and magnitude of velocity leads to the beta particles emitting electromagnetic radiation. The different energy losses per unit length for electrons in matter are given by Eqs. 5 and 6, similar to the Bethe-Bloch equation (Eq. 2) [4].

$$ \left(\frac{dE}{dx}\right)_c = \left(\frac{e^2}{4\pi\epsilon_0}\right)^2 \frac{2\pi N_A Z\rho}{m_e c^2 \beta^2 A}\left[\ln\frac{T\left(T+mc^2\right)^2\beta^2}{2I^2mc^2} + \left(1-\beta^2\right) - \left(2\sqrt{1-\beta^2} - 1 + \beta^2\right)\ln 2 + \frac{1}{8}\left(1-\sqrt{1-\beta^2}\right)^2\right], \tag{5} $$

$$ \left(\frac{dE}{dx}\right)_r = \left(\frac{e^2}{4\pi\epsilon_0}\right)^2 \frac{Z^2 N_A\left(T+m_e c^2\right)\rho}{137 m_e^2 c^4 A}\left[4\ln\frac{2\left(T+m_e c^2\right)}{m_e c^2} - \frac{4}{3}\right], \tag{6} $$

where subscripts c and r represent collision and radiation energy losses, respectively, and T is the beta particle kinetic energy. The radiative energy losses are only valid for electron energies above 1 MeV; for lower energies, bremsstrahlung is negligible.

A different kind of decay which does not involve change in nucleon numbers is 'gamma decay'. Nucleons are filled in the nucleus in fixed, discrete energy states, separate for protons and neutrons and the filling follows Pauli's exclusion principle [5]. Some nucleons can occupy

high energy levels even when some empty or partially filled lower energy levels exist, leaving the nucleus in an excited state. The nucleus can then de-excite to a lower energy state by emission of a gamma photon carrying away the energy. Gamma decay commonly follows other decays such as alpha or beta decays [6].

A phenomenon that directly competes with gamma-ray emission is internal conversion. In this case, the nucleus interacts electromagnetically with an orbiting electron (usually in the K or L-shell), transferring its excitation energy to it. The binding energy of the electron which holds it in the atom is usually much lower than the energy it got transferred from the nucleus and so it is energetic enough to leave the atom, leaving an unfilled electron orbital. Unlike in beta decay, this ejected electron is not created in the decay process and so the electron is not referred to as a beta particle. In addition, the emitted electron energy will always be fixed. Generally, following internal conversion (IC), an atomic electron in a higher energy shell will de-excite and occupy the empty lower energy orbital releasing energy (this is atomic relaxation); this energy is usually released as X-rays but can also be released by emitting a second atomic electron, referred to as Auger electron [6].

Photons are neutral, electromagnetic radiation and interact with matter differently from charged particles ionizing in the same energy range. Interactions include the photo-electric effect, Compton scattering, and pair production. Stopping ranges are much longer than for alpha particles or electrons. The detectors used in this thesis work are too thin for significant interaction with gamma and X-rays so their interaction processes are not discussed further here.

3 Semiconductor Detectors

The work in this project concerns the double-sided silicon strip detector DSSD – a Si-based, crystalline, semiconductor detector – that allows determination of the energy and position of an incident charged particle very accurately. In this section, the theory of semi-conductors and how they can be made to detect ionising radiation is discussed.

3.1 Semiconductor basics

To understand how semi-conductor detectors for ionizing radiation work, it is good to take a look at the basics of semiconductors. Here, atomic excitation, where electrons change in energy levels, is of relevance. The atoms in any material have discrete energy levels which are filled by electrons starting from the lowest energy level leaving the atom in its ground state. Overlap of the electron clouds from the

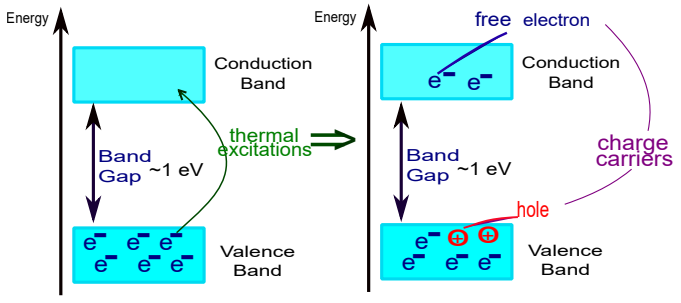

Figure 2: Energy bands and thermal excitation in a pure semiconductor.

individual atoms leads to the formation of energy bands which are a continuum of very close energy levels. The last filled energy band is known as the valence band and the band above that is known as the conduction band; this is illustrated in Fig. 2. In semiconductors and insulators, there is a range of energy values which do not correspond to any energy states, the forbidden region, known as the band gap. For a material to be conductive, it requires electrons in the conduction band (or a hole, i.e. an unfilled orbital, in the valence band) but in semiconductors and insulators this valence band is completely filled while the conduction band is empty. However, the band gap in semiconductors is small enough , ≈ 1 eV in the Si crystal lattice, such that at room temperatures, some electrons can be thermally excited to the conduction band leaving a hole in the valence band (see Fig. 2). Both the 'free' electron in the conduction band and the hole act as charge carriers in the material but the conductivity is still very low for most practical applications.

3.2 Doping

To make the semiconductors functional as detectors, certain impurities – referred to as dopants – are added to the semiconductor materials, a technique commonly known as doping. To see the effect of doping, take for instance, a silicon atom which has four valence electrons and all participating in bonding with neighbouring atoms. Now, as shown in Fig. 3a and Fig. 3b, by introducing a valence-3 or a valence-5 atom in the material, there will be a non-bonding electron due to a deficiency or an excess of one electron, respectively. This non-bonding electron will occupy energy levels in the once forbidden region in pure semiconductors. The excess electron from doping with valence-5 atoms results in donor levels close to the conduction band while the vacancy of an electron from doping with valence-3 atoms results in acceptor levels close to the valence band; this is shown in Fig. 3c. Electrons in donor levels can move to the conduction band while holes can be created in the valence band as electrons move to the acceptor levels. This happens much more easily due to the electrons having to cross the lower energy gap; see Fig. 3c. The excess of electrons in the conduction band (referred to as free electrons) makes the doped material n-type with the negative charged electrons being the primary charge carriers. Similarly, an excess of holes makes the doped material p-type with the positive holes being the main charge carriers.

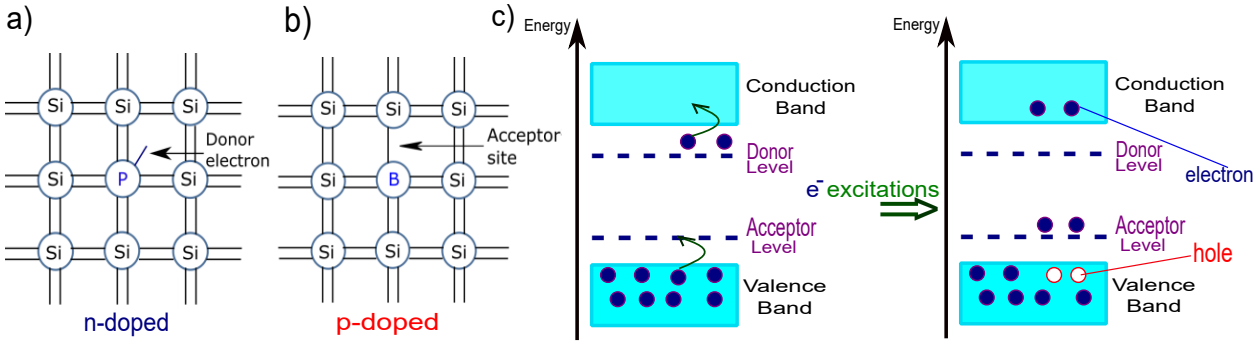

Figure 3: a) n-type doping leads to donor electrons [7]. b) p-type doping creates acceptor sites [7]. c) Presence of donor and acceptor levels in doped material allows easier excitations.

3.3 p-n Junctions and Ionizing Radiation Detection

To carry out measurements of ionising radiation, a so-called p-n junction comes into play. When a p-type material is brought in contact with a n-type material, the free electrons in the 'n-side' can travel and combine with the holes in the 'p-side'. This process, known as radiative recombination, creates a depletion region where no free charge carriers are present. As the electrons travel from the n-side to the p-side, there is a net positive charge and a net negative charge on the ends of the depletion region at the n-side and p-side, respectively. This results in an intrinsic electric field that prevents further recombination. When ionising radiation incidents on the depletion region, electron-hole pairs are formed. Figure 4 illustrates the formation of the depletion region and formation of electron-hole pair due to ionizing radiation. The electric field causes the negative electrons to flow in one direction while the positive holes in the other direction. This flow of charge carriers causes a current pulse that has amplitude proportional to the energy deposited by the ionizing particle. Application of a reverse bias, i.e. connecting the negative terminal of an external voltage supply to the p-side, results in an increase in the size of the depletion region. This has two advantages. First, the bigger depletion region means a greater region over which an ionizing particle can be detected is achieved. Second, the electric field across the depletion region is stronger and thus the charge collection is more efficient [4].

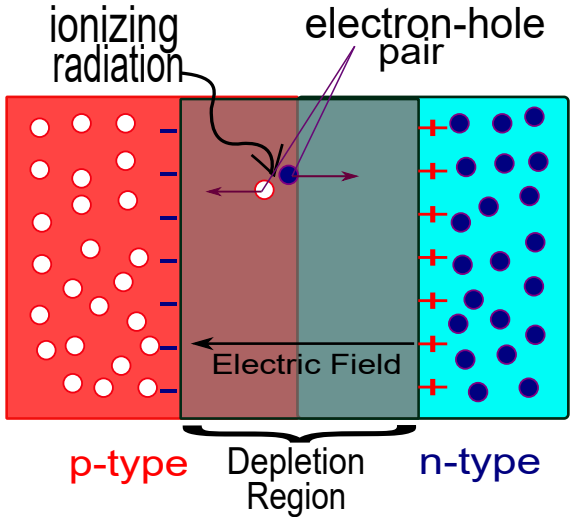

Figure 4: p-n junction, depletion region and detection of ionizing radiation.

4 Lundium

The Lundium decay station has been designed for the purpose of investigating rare, short-lived unstable isotopes – in particular, those in the superheavy region at the far end of the periodic table – behind separators, and for understanding their properties and nuclear structure from their spectroscopic analysis. Lundium – the next generation replacement of the TASISpec [8] decay station– has several new features added and old parts are upgraded making it the decay station that will allow measurements with the highest spectroscopic quality possible when completed.

4.1 Lundium Components

A 3-D render of Lundium is presented in Fig. 5. The central part of the decay station and the first detector that the directed beam sees is the implantation detector – a 58 × 58 strip, 300 μm thick DSSD – into which an evaporation residue 'EVR' – the resulting nucleus

formed after an energetic reaction – will be implanted. Behind the IMP DSSD, sits the veto detector, a twin DSSD of the implantation detector. Four additional 32 × 32 strip, 500 μm thick DSSDs are placed upstream of the IMP DSSD around its four corners forming a box-like setup; in essence, an open 'Si Cube' for detecting charged particles [9].

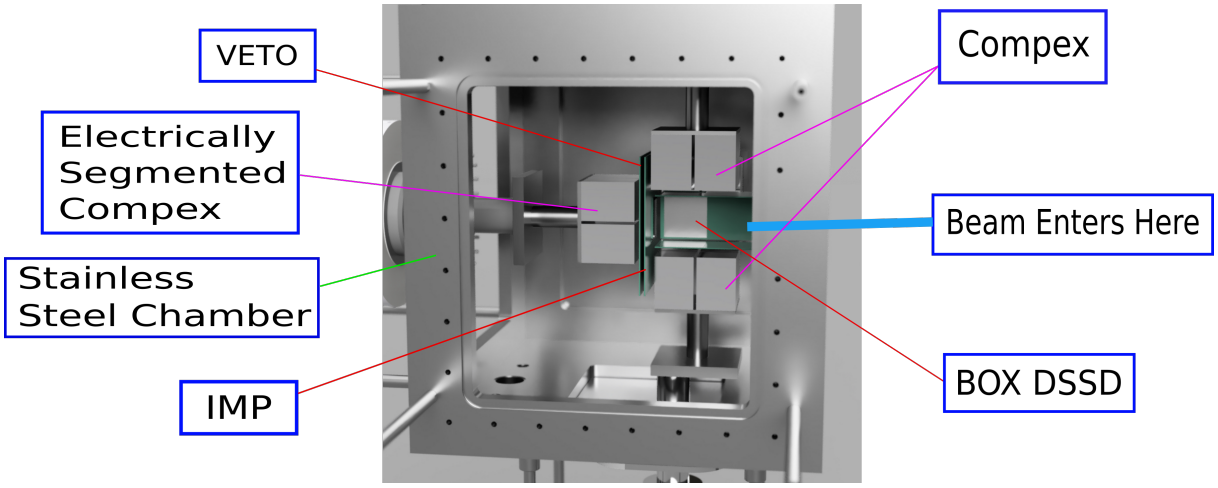

Figure 5: A rendered model of the Lundium Decay Station [10]. The Compex and box detector facing out of the page has been omitted here to make visualisation of the inner part better. The BGO shielding is also not shown here.

The unique Compex Germanium detectors, which boost the charge particle-photon coincidence efficiency are positioned right behind the silicon detectors in the Si cube [11]. Four Compex Ge detectors surround the four 32 × 32 box DSSDs while a fifth, electrically segmented, Compex – with four electronic segments for each of the four Ge crystals within it – stands behind the implantation-veto set-up [9]. When the decay station will be active, a vacuum will be created inside the chamber – made of thick, stainless steel to make it robust; this vacuum allows the germanium crystals to be used without the aluminium end-caps, reducing energy absorption of incoming photons in the caps before they reach the Ge crystals. This use of the Ge detectors allows enhanced photon detection efficiency, very significant for detecting low-energy gamma rays, or X-rays emitted following internal conversion. Last but not the least, an active anti-Compton shielding – consisting of bismuth germanate, BGO, crystals – borders around the Compex detectors to be able to cut down on background signals even more [12]. This design, with its very sensitive and selective detector system, will allow the best charge particle-photon coincidence detection efficiency and is undoubtedly going to become an invaluable tool in studying exotic nuclei.

4.2 The Double-sided Silicon-Strip Detectors

A DSSD is a semiconductor detector which consist of a thin silicon wafer passivated by silicon dioxide, and has floating guard rings to aid it to undergo complete depletion [13]. An aluminum layer is deposited on the wafer to improve electrical conductivity and quicken charge collection. The DSSDs relevant in this thesis work are the identical implantation and veto detectors. The silicon wafers in these are 320 μm thick and have a 60.1 mm × 60.1 mm

square shape. The active area on the DSSD is 58.5 mm × 58.5 mm. One (front) side is the junction or p-side while the other (back) is the ohmic or n-side; both sides have 58 strips.

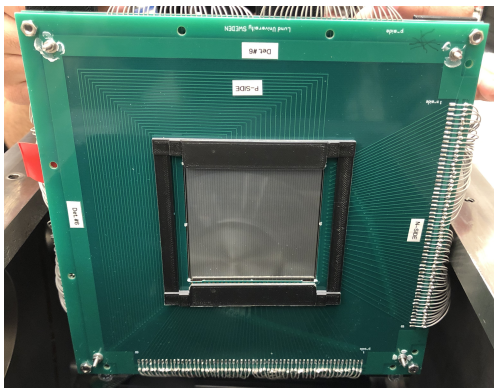

Figure 6: The 58-strips DSSD for the implantation detector supported on a PCB.

The p-side strips have a pitch, i.e. the distance from start of one strip to start of the next strip, of 1 mm, and an interstrip SiO_2 separation of ≈7.5 μm. The n-side strips which are arranged perpendicularly to the p-side strips are surrounded by an additional heavily doped p-type zone; this enhances interstrip capacitive and resistive isolation of the neighbouring n-side strips. Thus, the pitch size of these n-strips is also 1 mm, but the interstrip separation is much shorter than for the p-strip [14]. The orthogonal arrangement of the p-strips with respect to the n-strips creates a virtual grid of 'pixels' which will make two-dimensional tracking ($x - y$ positioning) of the incoming and decaying particle possible [15]. To ensure the DSSD is totally depleted, a reverse bias of about -40 V needs to be applied. The DSSD will also have a 'dead layer' of (mostly) silicon dioxide where ionizing particles cannot form electron-hole pairs to register energy and so some of the energy deposited is not detected; this dead layer which needs to be determined before Lundium launches becomes very important when calculating the full energy of alpha particles escaping the IMP DSSD [7].

The silicon wafers for the DSSD, delivered from RADCON Ltd, require preparation for use in experiments. In the preparation, the DSSD is placed on a FR4 frame and the whole set-up is transferred to a stainless steel holder and thin gold wires are used to connect the gold-plated pad on a printed circuit board (PCB) to the aluminium surface on the detector, in a process known as bonding. Silver glue-epoxy is used to secure the 'bonds' i.e connections. Pin-like connections are then tin-soldered into the holes in the frame. Finally, this entire structure is removed from the stainless steel holder and mounted on a PCB ready for use [14][15].

5 Veto Detector

5.1 Vetoing

As mentioned earlier, after an evaporation residue implants in an implantation detector, the implanted nucleus can undergo several of the different radioactive decays. Investigating these decays allows one to identify and get information on the nucleus. The decay method is determined by analysing the energies deposited in the different detectors in the – typically – many millions of events. The process of vetoing allows differentiation between different kinds of events, removal of unwanted background radiation, and overall have more clean final data to analyse; in essence, the selectivity of events is improved.

5.2 Lundium's Veto Detector

In the Lundium decay station, the vetoing process relies primarily on the Veto DSSD. Simply, this is a replica of the IMP DSSD positioned directly behind it, with a separation of 0.5 cm, while rotated 180°, so the p- and n-strips numbers increase antiparallel to those on the IMP DSSD. The presence of this Veto DSSD allows one to scan the ionizing particles that are able to pass through the implantation detector giving an idea of the type of particles that registers energy in just the IMP DSSD, or in both the IMP and Veto DSSDs.

5.3 Importance of Vetoing

In fusion experiments of exotic nuclei studies, a beam of heavy ion particles bombards on a heavier target material, a compound nuclei – with proton and neutron number close to the nuclei of interest – is created. The 'filtered' beam – filtered with separators using He gas and dipole plus quadrupole magnets – containing the fusion evaporation residue will be transferred to the decay station, where it gets implanted for spectroscopic measurements. The incoming beam can also contain light ions. The implants can decay further, for instance by alpha or beta decays.

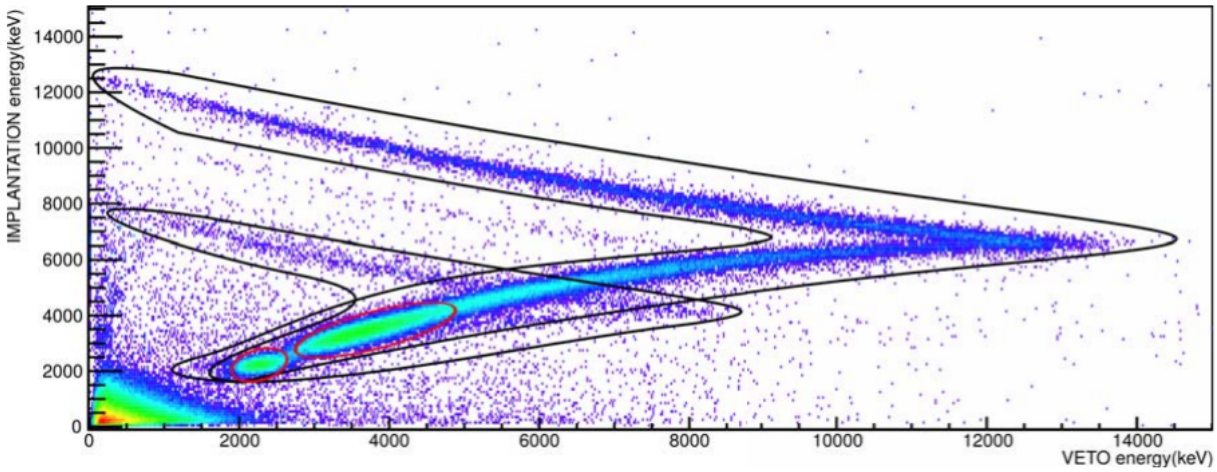

Figure 7: A particle identification plot by looking at IMP and Veto DSSD energies [16].

The energy deposition recorded by the DSSD depends on the particle type, its speed and the detector thickness. Hence, by looking at the energies registered on both the IMP and Veto DSSDs and correlating them to individual events, one can distinguish between light ion punch-through events, heavy-ion implantation events, or alpha decay events. An example of an implantation-veto particle identification plot, used in the spectroscopic studies of element 114, flerovium, decay chains is displayed in Fig. 7. In the plot, the black 'boomerang' shapes are due to scattered beam and target-like particles with the edge of the boomerang indicating 'punch' through both the IMP and Veto DSSDs. Red rings are scattered separator gas (He) which deposit about 2-4 MeV of energies in the IMP or Veto DSSD as they punch through; these would appear as escaping alphas without the use of both IMP and Veto

DSSDs [16].

When the implanted ion undergoes alpha decay, the alpha particle will likely deposit all its energy in the implantation DSSD or deposit some of it and recoil into one of the box DSSD, in which case the alpha particle can be 'reconstructed' using the energy deposition data on the Si-cube setup. However, at times the alpha particle may escape by recoiling back in the incoming beam direction; in which case, the low energy deposited by the alpha can be indistinguishable from an electron event. The presence of the veto detector enables the possibility to pick out these escaping alphas from the electrons since the electrons punch through the implantation DSSD; unless the electron has very low energy, in which case, it cannot be considered as an alpha anyway and it is interpreted as a potentially 'real' electron.

6 Assessment of Vetoing Capability

In this thesis work, the implantation plus veto detector back-to-back setup was put to the test to observe how well one can correlate two hits (where a 'hit' is defined a coincidence of almost identical energy deposition on p- and n-side strips of the detector), one in the implantation and one in the Veto DSSDs, to be from the same electron event within a high level of confidence when vetoing beta-decay events. Carrying out this investigation involved setting up the necessary physical equipment, having a detector control and data acquisition system, as well as performing online monitoring of the data being recorded. Once data taking was complete, the next steps were reading the recorded data offline, checking to get quality assurance, mapping it into the relevant coordinates, and doing data analysis. Data was taken with a standard electron source placed at a known distance for a sufficient time period. Once the data taken was checked for quality, it was used to build the distributions of the energy hits on the two detectors and then interpreted. The rest of this section discusses in depth the methodology used to undertake this.

6.1 Experimental Setup & Data Acquisition System

In Figs. 8 to 10, the different parts of the experimental set-up are highlighted. The stainless-steel chamber encases the IMP and Veto DSSDs back-to-back set-up as well as the electron-source. For data taking, the p- and n-strips in a quadrant of each DSSD, covering the same real x-y coordinates, were selected. This was the top-right corner of the DSSDs, as shown in Fig. 9, consisting of strip-numbers 1-29 on both p and n-sides for the implantation DSSD and strip-numbers 30-58 on both p and n-sides for the Veto DSSD. These selected strips were cabled to four, 32 channel preamplifiers (produced by IKP, Cologne) for reading out the current pulses, i.e. energy signals, in each and every one of those strips [13]. Half of the channels, 16, read by each preamplifier are connected to one FEBEX3 card; 8 FEBEX3 cards, numbered 0-7 as shown in Fig. 11, connect all the required electronic channels [17].

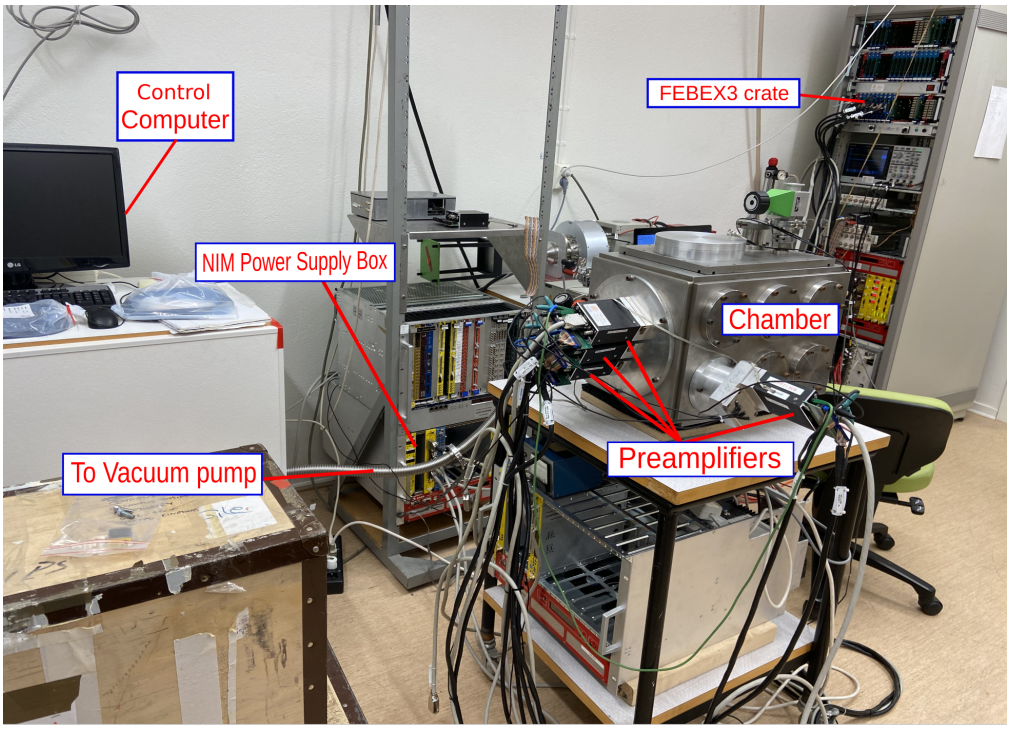

Figure 8: The experimental set-up used to collect data. The readout computer, the EXPLODER card and the digital pressure gauge are not visible in the image but are connected.

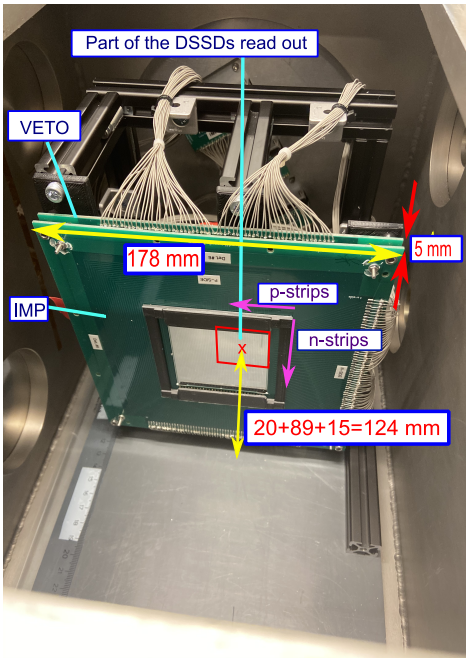

Figure 9: Only a quadrant of the DSSDs (indicated by the red square) was cabled for data taking.

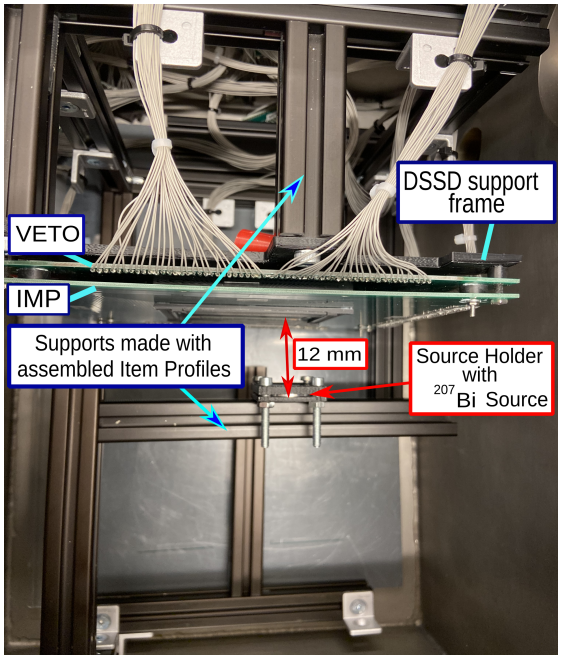

Figure 10: The set-up in the chamber with its key features shown.

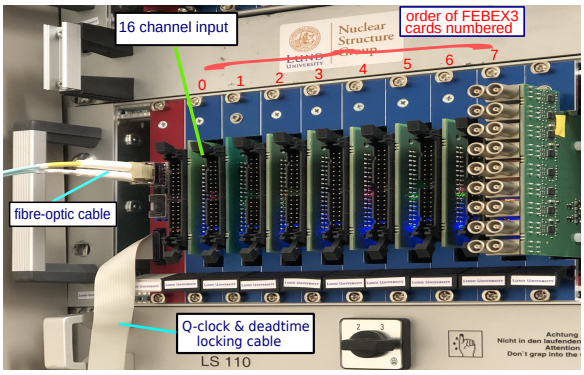

Figure 11: The FEBEX3 digitizer card crate with the cards' assigned card numbers.

A ^{207}Bi electron-source (where the emitted electrons are a result of internal conversion) was used to irradiate the relevant detectors' quadrant. The source was positioned with the aid of a stable support assembled using a number of item© profiles; three of the item© profiles were arranged all orthogonal to each other allowing to situate the source holder and hence the source in any desired position in space within the chamber. In this work, the source is kept at a very short distance of $\approx$ 1.2 cm from the detectors such that it reasonably mimics an implanted nucleus, while at the same time being cautiously away from the detector surface.

Once the inside of the chamber was all set up and the position measurements recorded, a vacuum pump is used to evacuate the air inside to reach a reasonable vacuum – monitored using a digital pressure gauge. The detectors are then reverse biased with a voltage of $-$ 40 V, while a voltage of $-$ 5 V is used to power the preamplifiers. The voltage is supplied by connecting to a high voltage NIM power supply box. As energy from ionizing radiation is absorbed in the detectors, a current pulse is produced which induces a corresponding voltage on the preamplifiers, proportional to the energy deposition.

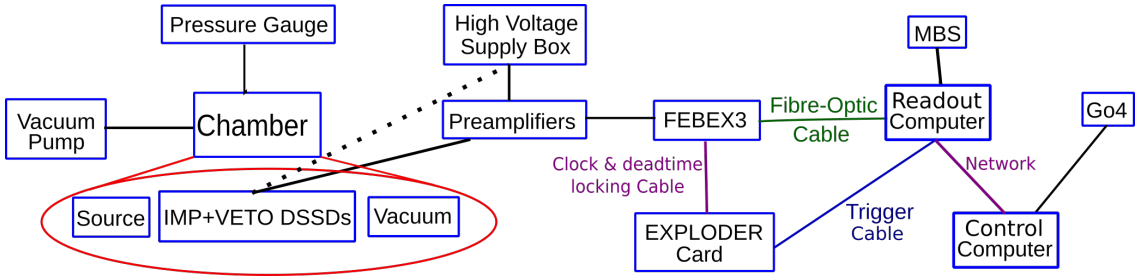

Figure 12: The experiment schematics. The red circle indicates the modules that are present inside the chamber. The high voltage supply box supplies the -40 V for reverse biasing the detector through connections in the preamplifiers rather than directly.

Figure 12 shows schematically how the experimental set-up and data acquisition are connected. The preamplifier signals are constantly being sent to the FEBEX3 [17] digitizer cards, sampling at a rate of 50 MHz. These FEBEX3 cards digitize the analog voltage pulses they get from the preamplifiers into a computer readable and storable form. The FEBEX3 crate is further connected to so-called EXPLODER card, through a 'clock & deadtime locking' cable, and a readout computer – where a multibranch system (MBS) data acquisition software runs for sorting energy signals, i.e. 'events' – through a fibre-optic cable. The EXPLODER card is also connected to the readout computer, and checks whether it is 'busy' or not – that is whether an event is currently being recorded or is the readout computer free to start recording a new event – and then 'notifies' this status to the FEBEX3 cards. When an

interesting energy signal, above a certain set threshold, is detected by the FEBEX3 cards and the readout computer is not flagged as busy, the digital energy signals are sent to the readout computer which initiates the start of recording an event. The recorded event represents a voltage pulse seen over a set time interval. Every one of these event signals seen are sent to a control computer where histograms of the energy signals sorted for each channel are produced with the use of Go4 [18], a ROOT-based software that is suitable for plotting data. The control computer allows easier data monitoring and analysis. Online data monitoring is done using Go4 to check whether the data being recorded makes sense and there are no indications of faulty equipment or incorrect setup. A copy of all the events are stored in a secure network disk for offline data analysis once the data taking is done [19].

6.2 Data Analysis

To begin the data analysis, one must first unpack the data which comes from MBS as a listmode binary data file 'lmd' and store it as a more meaningful ROOT-tree. This ROOT file will have the raw uncalibrated FPGA (Field-Programmable Gate Array) energies, represented as 'channels' until calibrated, and times of all the events recorded by the FEBEX3 digitizer cards. Each channel corresponds to a strip on the DSSDs. With the cabling of the detector strips to the cards known, the 128 channels read by the FEBEX3 cards can be mapped into p- and n-strip numbers. If there were any errors in the cabling, the mapping will show different-than-expected hit patterns from which the correct mapping might possibly be worked out; otherwise, it might require further investigation into the cabling and connections.

Once the mapping to strips was properly achieved, histograms of the full hit distributions on the IMP and Veto DSSD were made pixel by pixel in 'p-n space'. This involved checking the energy deposited in a single p-strip and comparing it with the energies deposited on the n-strips, within a short time interval of 1 μs. If the energy in one of the n-strips was close to the energy in the p-strip, a 'pixel hit' was formed effectively giving the position of the ionizing particle in the DSSD. With the pitch of the DSSDs and total strip numbers known, the hit distributions were mapped in '$x - y$' coordinates to visualize the data in 'real space'.

The hit distributions seen on the IMP and Veto DSSDs in real space (x, y) coordinates were plotted and their projections on x and y were used to determine the centers of the distribution with the help of fitted Gaussians. The centers of the spread seen on the two DSSDs were then used to double check whether one can reconstruct the center of the electron source. To reconstruct the source center, the parametric equation of the straight line passing through the spread centers on the DSSDs were derived. The point at which this line intersects the plane containing the face of the electron source was then found; this is the reconstructed center. Figure 13a illustrates the procedure with the necessary distances, points and planes used.

The next part, which is the main part in assessing the vetoing capability, involved seeing the Veto DSSD hit distributions formed by gating on certain pixels hit on the IMP DSSD. The selected pixels included a central pixel (p,n)=(15,15), off-center pixels (p,n)=(11,11) and (8,8), end strip pixel (p,n)=(14,3) and lastly edge pixels (p,n)=(3,3) and (2,2); these

different pixel types are illustrated in Fig. 13b. The four selected kinds of pixels should allow to illustrate all the different possible spread of the electron hits on the Veto DSSD for any electron hit position on the IMP DSSD.

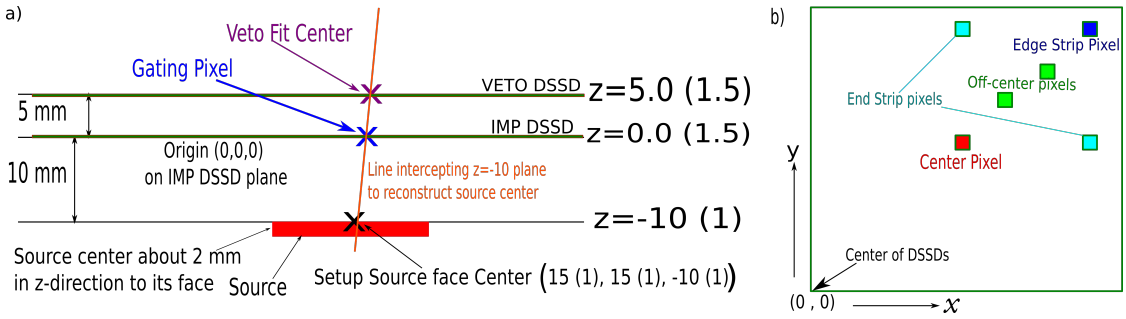

Figure 13: a) Top view sketch of source & detector setup for center reconstruction using the IMP and Veto DSSD hits. b) General positions of the different gated pixel types in $x-y$ space.

Once the gated distributions were plotted, Gaussian functions were fitted to the projections of the plots on both x and y directions. All the Gaussians were fitted using Go4 software. The source center was reconstructed using the peak centroids of these fits for each gated pixel for verification. Finally, the standard deviations σ from the Gaussian fits were found for each of the selected pixels.

7 Results

Figures 14 and 15 show the total hit distributions, when using the ^{207}Bi electron source, recorded with the IMP and Veto DSSDs, respectively, in $x-y$ coordinates. The figures show that the electron distribution is more spread out as well as having lower total counts on the Veto DSSD relative to the IMP DSSD.

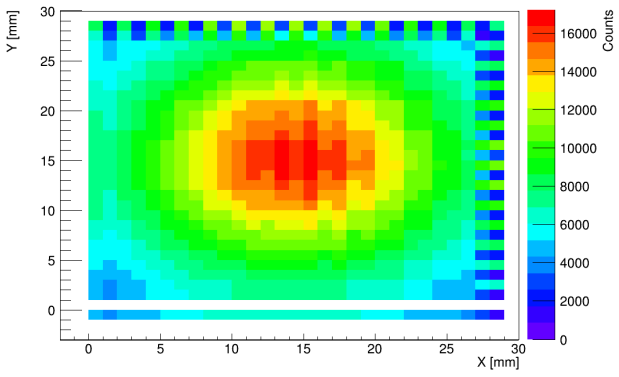

Figure 14: 2D pixel hit map of the total hit distribution recorded by the IMP DSSD in $x-y$ space. There is a blank channel seen caused by skipping of a channel due to issues in the DSSD PCB connections. Details in section 'Cabling & Skipping of channels' in the Appendix

.

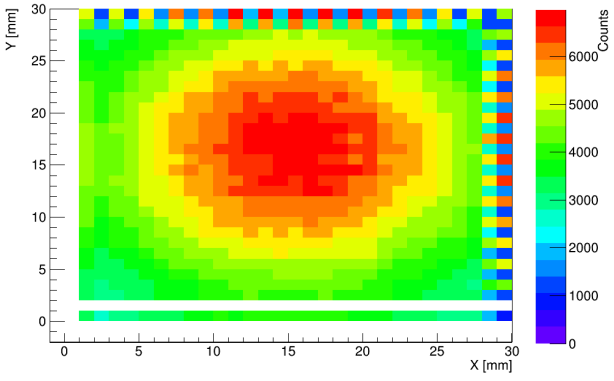

Figure 15: 2D pixel hit map of the total hit distribution recorded by the Veto DSSD in $x-y$ space. Both the IMP and Veto DSSD hit maps show uneven, very noisy pixels at the detector end strips; a result of inefficient charge collection at these strips.

Veto DSSD hit distributions produced by gating on the four different pixel types considered are displayed in Figs. 16 to 19. The centers of these distribution correspond closely to the gated IMP DSSD pixel as a 'source'. The maximum counts can be seen to get increasingly lower as one gates on pixels further away from the source center. From gating on end pixels, one only sees a proper Gaussian like distribution in one direction (x or y), while gating on edge pixels barely show any sort of normal distribution; the counts are also very low.

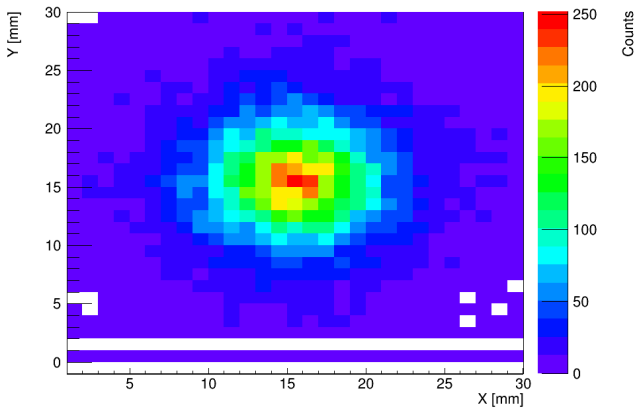

Figure 16: Veto DSSD hit distribution from a gated center pixel. (x, y)=(14.5, 14.5) [mm].

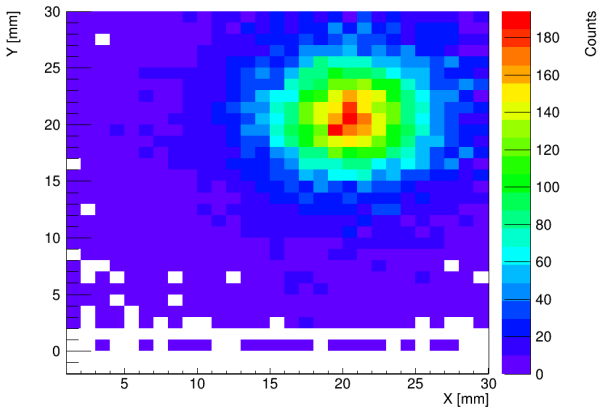

Figure 17: Veto DSSD hit distribution from a gated off-center pixel. (x, y)=(18.5, 18.5) [mm].

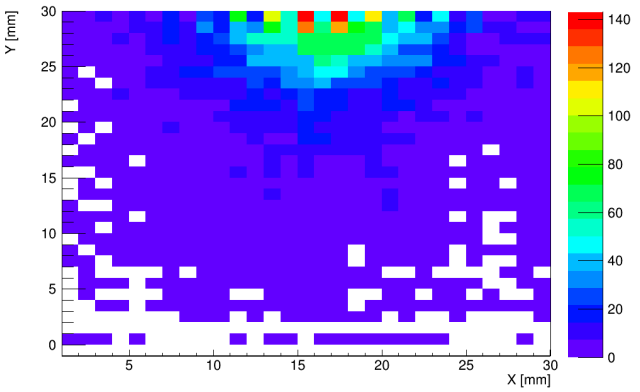

Figure 18: Veto DSSD hit distribution from a gated end strip pixel. (x, y)=(15.5, 26.5) [mm].

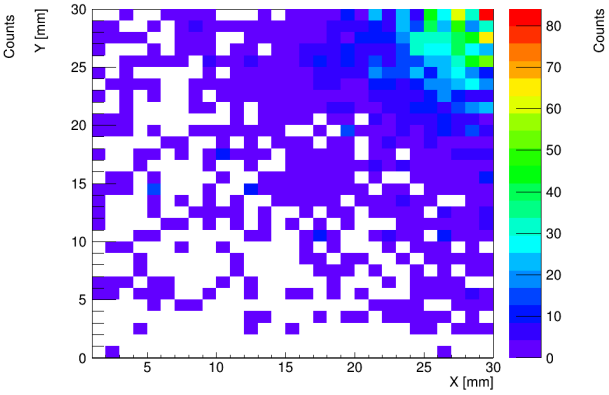

Figure 19: Veto DSSD hit distribution from a gated edge pixel. (x, y)=(26.5, 26.5) [mm].

The Gaussian fits for the projections on x and y direction for the gated center pixel distributions and an end strip pixel are presented in Figs. 20 to 23, providing examples of how the projection of the distribution and the Gaussian fits look like. As shown in Fig. 23, the distribution in one projection direction (or even both) might not show a maximum peak and a normal distribution on which a Gaussian fit can be performed; no fits were performed on these kind of cases.

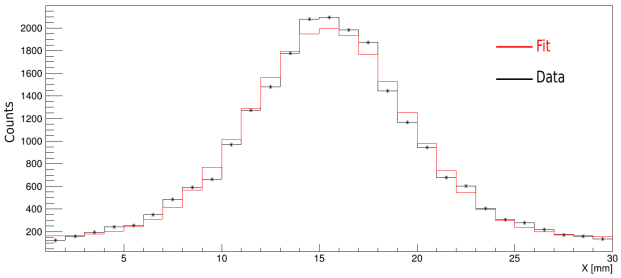

Figure 20: Projection of the distribution on x direction along with its Gaussian fit from the gated center pixel.

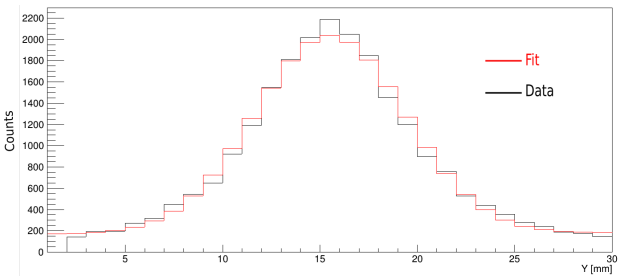

Figure 21: Projection of the distribution on y direction along with its Gaussian fit from the gated center pixel.

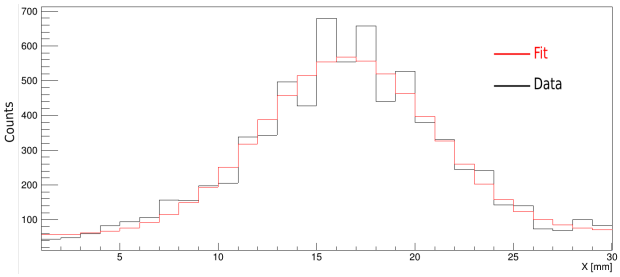

Figure 22: Projection of the distribution on x direction along with its Gaussian fit from the gated end strip pixel with (p,n) = (14,3).

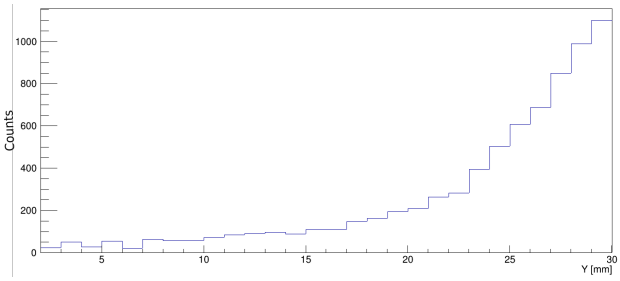

Figure 23: Projection of the distribution on y direction from the gated end strip pixel with (p,n) = (14,3). In this case, it was not reasonable to fit a Gaussian function to the distribution.

Table 1: Reconstructed source center result from the full IMP and Veto DSSD hits. Values in [mm].

	(x , y , z)
Full IMP Fit Centroid	(14.42 (1.02) , 15.34 (1.02) , 0.0 (1.5))
Full Veto Fit Centroid	(15.94 (1.11) , 17.33 (1.11) , 5.0 (1.5))
Reconstructed Source Position	(11 (4) , 11 (4) , − 10 (1))
Setup Source Center	(15 (1) , 15 (1) , − 10 (1))

Table 1 shows the data used and the results for the reconstructed source center using the total hit distributions recorded by the DSSDs. Table 2 shows the fit centroids found in the Gaussians of the hit distribution projections from gating as well as the source center coordinates reconstructed from the gated pixel location and the fit centroid values.

Table 2: Pixel Types Gated and corresponding reconstructed source centers. 'No fit' values cannot be reconstructed.

Pixel Type	**IMP Pixel Hit** (x_1, y_1) ± (0.5, 0.5) [mm]	**Veto Fit Centroid** (x_2 , y_2) [mm]	**Reconstructed Center** (x_3, y_3) [mm]
Center	(14.5 , 14.5)	(15.43 (1.04) , 15.52 (1.04))	(12.6 (2.8) , 12.5 (2.8))
Off-Center	(18.5 , 18.5)	(20.28 (1.05) , 20.48 (1.05))	(14.9 (3.2) , 14.5 (3.4))
	(21.5 , 21.5)	(23.89 (1.06) , 23.92 (1.06))	(17.0 (4.0) , 17.0 (4.0))
End Strip	(15.5 , 26.5)	(16.54 (1.08) , no fit)	(13.4 (2.9) , no fit)
Edge	(26.5 , 26.5)	no fit	
	(27.5 , 27.5)	no fit	

Table 3: Standard deviation σ values for the different Gated Pixels. Omitted values where Guassian fits were not possible.

IMP Pixel Hit (x_1 , y_1) ± **(0.5, 0.5) [mm]**	**Veto Dist.** σ_x **[mm]**	**Veto Dist.** σ_y **[mm]**
(14.5 , 14.5)	4.00 (0.04)	3.86 (0.04)
(18.5 , 18.5)	3.85 (0.07)	3.63 (0.06)
(21.5 , 21.5)	3.84 (0.09)	3.53 (0.09)
(15.5 , 26.5)	4.33 (0.10)	–
(26.5 , 26.5)	–	
(27.5 , 27.5)	–	

The uncertainty in the coordinates of the setup source position is dependent on the precision on the scale used when positioning it in the desired place. The z-coordinates of the DSSDs have uncertainties dependent on the thickness of the PCB support where they are placed within. The gated pixel hits on the IMP DSSD have uncertainties corresponding to the strip pitch, while the uncertainty in the fit centroids used as coordinates were regarded as a combination of the uncertainty from the fitting plus the pitch of the strips; the size of the pitch is added to the fit centroid uncertainty since the fit alone does not really give the exact position of the maximum as the fit is also performed using the energy deposition over a whole strip spanning 1 mm across.

Table 3 presents the final and key results of this thesis work – the standard deviations, σ_x and σ_y, of the Gaussian distributions seen in the Veto DSSD hit distribution from gating on

selected pixels. The standard deviations, which are the sigma values for a Gaussian function, for the edge pixels and part of the end strip pixels are not applicable since its not possible to perform proper Gaussian fits on the distribution seen in them. The uncertainties in the σ values come from the fit performed using the Go4 software.

8 Discussion

From Figs. 14 and 15 for the total hits distribution for the IMP and Veto DSSD, one sees the centers of the spread are closely aligned and so the two DSSDs in the back-to-back setup are not seen offset of each other as expected if the source was centered properly as well. The spread of the distribution is larger on the Veto DSSD compared to the IMP DSSD illustrating how electrons travel at rather noticeable angles through matter rather than in straight lines. This is additionally due to the fact that for the same solid angle, the coverage is larger at longer distances. The number of counts are also much lower on the Veto DSSD meaning a large number of electrons have had most of their energies absorbed in the IMP DSSD. The solid angle seen by the full IMP DSSD is higher and this further leads to increased counts and more narrow distributions seen on the implantation detector. As shown in Table 1, the spread centers used to reconstruct the electron source center and the calculated result of $(x,\ y,\ z)$ = (11(4), 11(4), -10(1)) agreed with the actual setup source center of (15(1), 15(1), -10(1)) within the range of uncertainty. This verifies that the source was properly positioned to the center of the DSSD quadrant being investigated as intended. Table 2 further validates this as all the gated IMP DSSD pixels from which the center could be reconstructed gave a value within the margin of uncertainty as well.

From the 2D hit maps of the gated pixel distributions and Table 2, one sees that the centers of the distribution align with the gated pixel and the source center as well meaning the gating was performed with the intended pixel. Further away from the source center alignment, the gated distributions are seen to lose the general 'normal' distribution. This is because the angles are so steep that most of the electrons simply never reach the Veto detector after passing the implantation detector. This is especially true for the the edge pixels where barely any Gaussian distribution can be observed and furthermore the number of counts are very low.

Table 3 displays the main findings of this thesis work, which are the σ_x and σ_y values of the Veto DSSD distributions for the four kinds of gated IMP DSSD pixels that will allow determination of the electron spreads for any hit position on the implantation detector. The σ values in all cases where it was possible to calculate was about 4 mm corresponding to 4 pixels in the DSSDs used. The edge pixels can be seen to have no calculated σ and this indicates that it is not possible to reasonably label electron events here and perform proper vetoing. It should be best to take extra care when dealing with these edge pixels and it might even be better to simply ignore hits here rather than trying to label them. Another option for these kind of cases could be to use the value of 4 pixels for σ which was the general case. The Veto DSSD hit distributions from the gated center and off-center pixels are Gaussian and the standard deviations have been found with very low uncertainties of maximum ≈ 0.1 mm as seen in the table. These σ values that give the spread of the electron distributions will

allow to label and set apart electrons that are not in coincident positions for the IMP and Veto DSSDs from the similarly behaving escaping alpha events to a great degree of accuracy within a high confidence level when relevant in actual decay spectroscopy experiments.

9 Conclusion & Outlook

In conclusion, the project work discussed in this thesis has been a great success at assessing the vetoing capability of Lundium's veto detector at vetoing beta-decay events. The important theoretical background required for the work including the basics of ionizing radiation and semiconductor detectors have been discussed. The structure of the Lundium decay station and the motivation for study of its vetoing capability have been presented. The experiment performed has been described in detail and the results obtained are reasonable and shall be very useful for decay spectroscopy experiments carried out with Lundium. As a future outlook, the vetoing of the beta decay events using the electron source from a further distance, representing those coming from the beam line or the box DSSDs can be performed. One could also test vetoing with known implanted nuclei instead of an external electron source. Another interesting project would be to see whether vetoing of low energy photons which manage to deposit energy on the DSSDs need vetoing or can be vetoed if ever necessary.

References

[1] Y.T. Oganessian. Synthesis and decay properties of superheavy elements. Pure and Applied Chemistry - PURE APPL. CHEM. 78, 889-904; 2006.

[2] Kenneth S. Krane. Introductory nuclear physics. 2ed. New York : Wiley, cop. 1988. Chapter 6, Radioactive decay; p. 160-178.

[3] Kenneth S. Krane. Introductory nuclear physics. 2ed. New York : Wiley, cop. 1988. Chapter 8, Detecting nuclear radiations; p. 246-261.

[4] Kenneth S. Krane. Introductory nuclear physics. 2ed. New York : Wiley, cop. 1988. Chapter 7, Detecting nuclear radiations; p. 213-217.

[5] Esam M.A. Hussein. Radiation Mechanics. Oxford, Elsevier Science Ltd, 2007. Chapter 1, Mechanisms; p. 1-65.

[6] Kenneth S. Krane. Introductory nuclear physics. 2ed. New York : Wiley, cop. 1988. Chapter 10, Gamma decay; p. 341-347.

[7] E. Kosta. Dead-layer Determination for the new Implantation detector of the LUNDIUM Decay Station [BSc Thesis]. Lund University; 2022.

[8] L.-L. Andersson, et al., TASISpec [U+2010] A Highly Efficient Multi[U+2010]coincidence Spectrometer for Nuclear Structure Investigations of the Heaviest Nuclei. Nucl. Instrum. Methods. Phys. Res. A 622, 164; 2010.

[9] D.M. Cox et al., UNILAC Proposal: Discovery and Spectroscopy of Neutron-Deficient Pu Isotopes and their Alpha-Decay Daughters; 2020.

[10] Rendered CAD Images; Nuclear Structure Group Repository; 2021.

[11] A. Såmark-Roth et al., Compex: a cubic germanium detector. Eur. Phys. J A 56, 141; 2020.

[12] Y. Hrabar et al., Anti-Compton shield for COMPEX germanium detector modules. To be submitted to Nucl. Instrum. Methods, in preparation.

[13] P. Golubev et al., The Lund-York-Cologne Calorimeter (LYCCA): Concept, Design and Prototype Developments for a FAIR-NUSTAR Detector System to Discriminate Relativistic Heavy- ion Reaction Products. Nucl. Instrum. Methods. Phys. Res. Section A: Accelerators, Spectrometers, Detectors and Associated Equipment, 723, 55; 2013.

[14] P. Golubev. Private Communication, 2021.

[15] D. Farghaly. Characterization of Double Sided Silicon Strip Detectors from LYCCA modules for FAIR [BSc Thesis]. Lund University; 2019.

[16] D.M. Cox et al., Spectroscopic Tools Applied to Flerovium Decay Chains. J. Phys. Conf. Ser. 1643, 012125; 2020.

[17] J. Hoffmann. FEBEX3b, specification; `https://www.gsi.de/fileadmin/EE/Module/FEBEX/febex3b.pdf`; 2013.

[18] Go4 analysis framework; `https://www.gsi.de/en/work/research/experiment_electronics/data_processing/data_analysis`; 2021.

[19] L.G. Sarmiento. Private Communication, 2021.

[20] Fusion 360 — 3D CAD, CAM, CAE & PCB Cloud-Based Software — Autodesk; `https://www.autodesk.com/products/fusion-360/overview`; 2021.

A Appendix

A.1 AutoDesk Fusion 360

One of the preparations for carrying out the actual experiment involved making models of the different components to be used in the 3D Computer Aided Design (CAD) software 'AutoDesk Fusion 360' to ensure the detectors, source + source holder, item© profile supports, cables would fit and can be positioned nicely in the chamber [20]. Models for some of the components such as the IMP and Veto DSSDs, and their support frame were already available in the Nuclear Structure Group repository; thus, in this work only the experimental chamber, the source holder and the source holder support+positioning stand were newly designed. Renders of these three components are illustrated below (Figs. 24, 25, and 26).

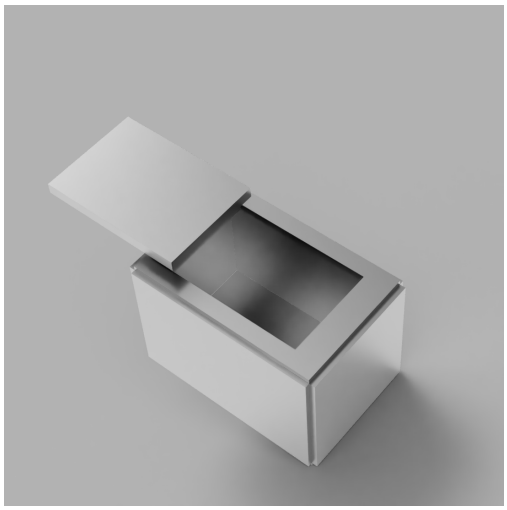

Figure 24: Simplified model of the experimental chamber.

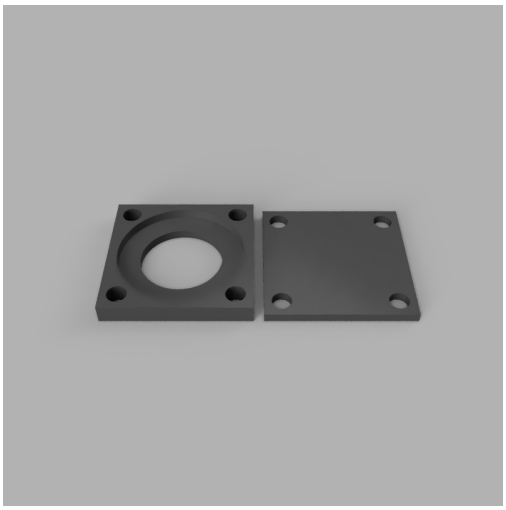

Figure 25: The rendered source holder used in the experiment.

Figure 26: Preliminary blueprint of the item© profile assembled support & positioning system. The base was altered during installation in the chamber during the actual experiment to make removing and putting the support back inside easier and safer.

As a side note, the 'AutoDesk Fusion 360 on a browser' version was used at the start of the work for the drawings – since it requires no installation of the software and still runs decently – however, later the procedure was switched to the AutoDesk Fusion 360 on the desktop, since the web browser version made drawings, editing, different angle viewing or combining components a lot time consuming and inefficient. It is definitely advised to stick to the desktop version if possible.

A.2 Hardware to Software Mapping

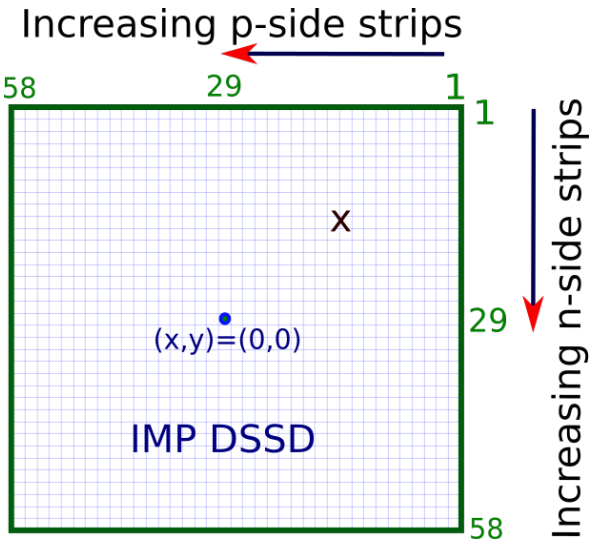

Figure 27: Sketch of how the p- and n-side strips are ordered when looking in face view of the IMP DSSD with respect to the source. The red square highlights the active (cabled) region during the experiment and 'X' represents the height at which the source was placed.

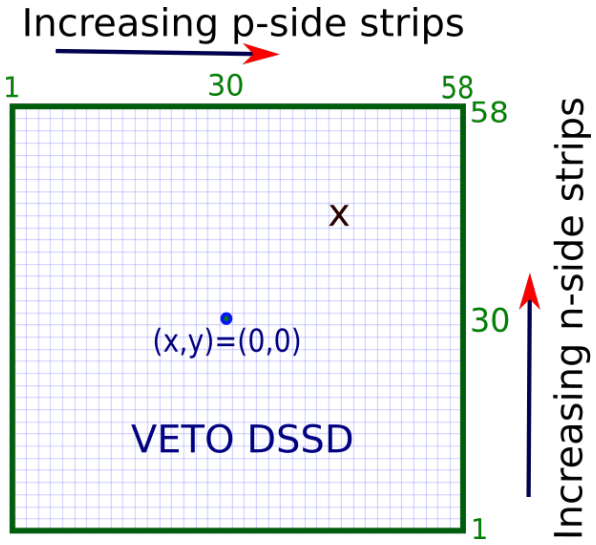

Figure 28: Sketch of face view of the Veto DSSD with respect to the source. The strips cabled consist of high numbers in the Veto DSSD compared to the IMP DSSD where low numbers were used.

The direction the p- and n-side strips increase is important to note down for converting the hit patterns in the detectors to real space coordinates in (x, y). The orientation of the IMP and Veto DSSDs are 180° rotated with respect to each other and so the strips do not increase the same way which one must keep in mind during data analysis. Sketches of the orientation of the two DSSDs as in the experimental setup and how the strips run in each are shown in Figs. 27 and 28. Taking the center of the DSSDs as the origin for the $x - y$ mapping, the $(x,\ y)$ coordinates along the DSSDs are easily calculated with knowledge of the pitch size and strip number. In Figs. 29 and 30, one can see the differences in the plots for the p-n and $x - y$ mappings. The $x - y$ mappings allow to visualise how the hit pattern take shape in the actual experiment more easily.

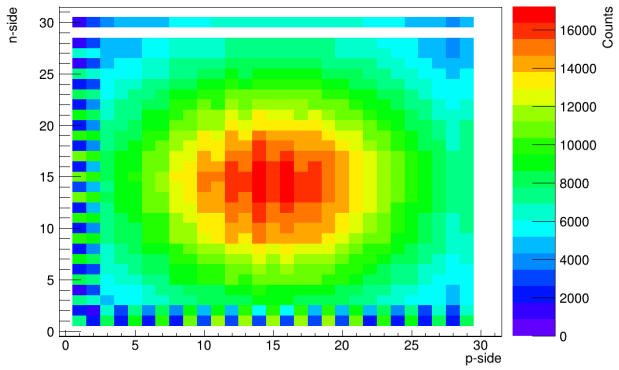

Figure 29: p-n mapping of the IMP DSSD hits. The strip numbers do not increase in the same direction as the plot's axes show here.

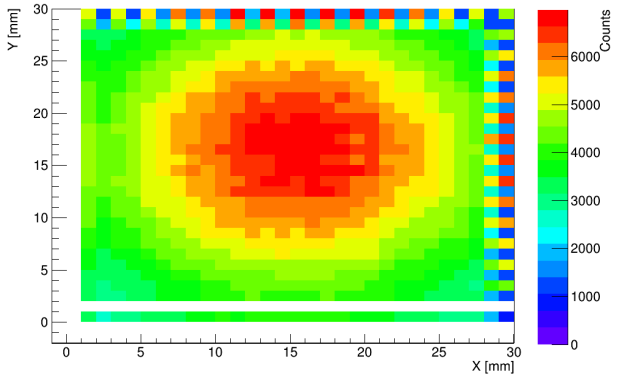

Figure 30: The x-y mapping plot for the IMP DSSD appears rotated 180° with respect to the p-n mapping plot, but conveys the same information.

A.3 Control of Data Quality

The raw data recorded by the FEBEX3 cards allows one to cross-check if the DSSD strips are cabled as intended and if the channels read are the ones intended and in the correct order. It also allows to see if any supposedly working channels were not giving any signals or if they were 'ringing'. In Fig. 31, the raw FPGA 2D hit pattern is shown where it can be seen that channels 0 and 15 in alternating cards are zero as intended. Moreover, the counts are increasing across channels in even (and 0) cards while the counts are decreasing along the odd numbered cards. With the source being centered with respect to the detector quadrant being measured, this shows agreement with how the DSSD strips were desired to be read by the cards. The one-dimensional histogram of the implantation and veto detector hits as a function of channels are also shown in Fig. 32 illustrating this.

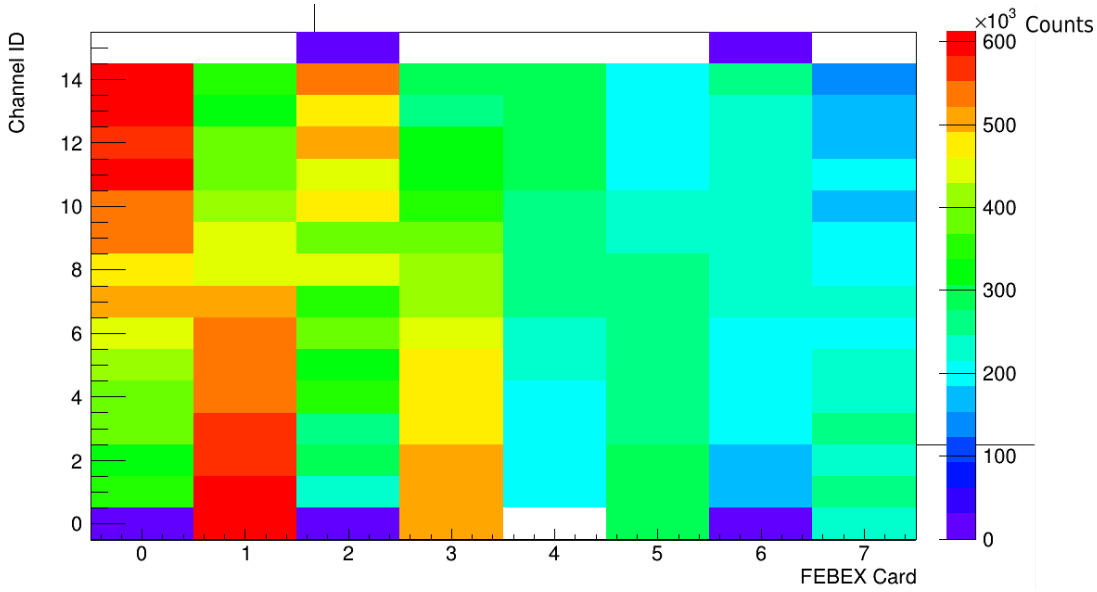

Figure 31: The Raw FEBEX3 FPGA hits

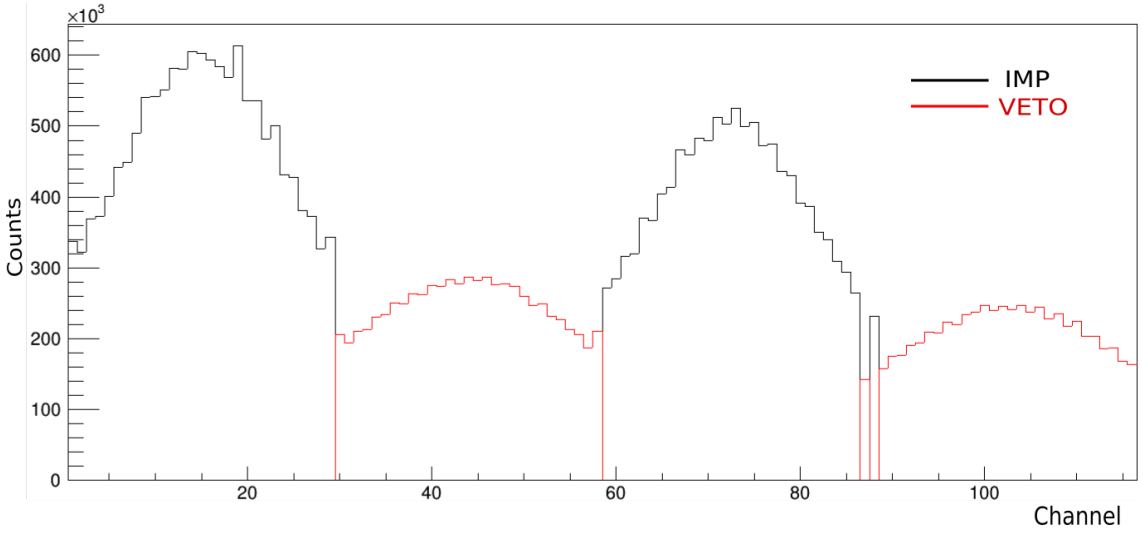

Figure 32: The 1D histogram of IMP & Veto DSSD hits seen as function of channels (correctly mapped from cards). The channel numbers are dependent of how the four preamplifiers are connected to the FEBEX3 cards.

A.4 Cabling & Skipping of channels

For the very first time, it can be challenging to make sense of the data read and configure the mappings from channels to p-n strip numbers when the cabling is not as expected. In this work, there were two important cabling issues noted that caused the correct mapping to be delayed. First, the preamplifier input were read in reverse (from high to low channel numbers) to the cards rather than initially thought; see Fig. 33. Second, the n-side strips were also being read in reverse but every two adjacent strips read were switched – an issue with the pin connections on the PCB board. This led to the blank channel as seen in the plots for the IMP and Veto DSSD hits; the switching resulted in the skipping of channel 29 (and using channel 30 instead) in the IMP DSSD and skipping of channel 30 (and using 29 instead) in the Veto DSSD.

The incorrect mapping was realised thanks to the use of a non-symmetrical 'mask' in front of the IMP DSSD and looking at the 'shadow' seen in the implantation detector's hit pattern. With the mapping first used, the shadow was not as expected, rather inverted and this motivated to further investigate the cablings and input channels for the preamplifiers and DSSDs, which after a rather longer than expected time, eventually lead to solving the issue; see details in E.Kosta's Bsc thesis [7].

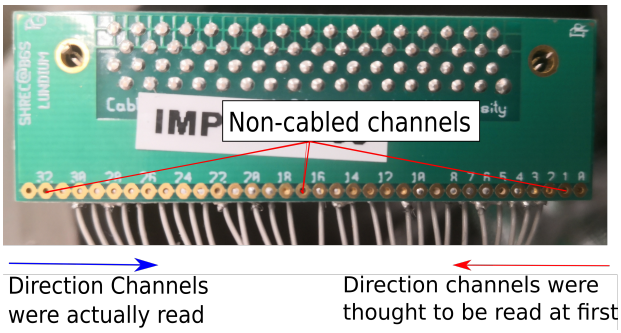

Figure 33: The PCB for the preamplifier input channels. Three of the channels are non-cabled to make up for the 58 p-/n-strips (rather than 64) on the DSSDs.